Origin of the photoemission intensity oscillation of C_{60}

Shinji Hasegawa, Takayuki Miyamae, Kyuya Yakushi, and Hiroo Inokuchi
Institute for Molecular Science, Myodaiji, Okazaki 444, Japan

Kazuhiko Seki
Department of Chemistry, Faculty of Science, Nagoya University, Nagoya 464-01, Japan

Nobuo Ueno*
Department of Materials Science, Faculty of Engineering, Chiba University, Inage-ku Chiba 263, Japan
(Received 17 December 1997)

The photon-energy dependences of photoemission intensities of C_{60} were quantitatively calculated by the single-scattering approximation for the final state and the *ab initio* molecular orbital calculation for the initial state. The calculated results agreed well with the measured intensity oscillation in the photon-energy range of $h\nu = 18-110$ eV. The calculation by the plane-wave approximation for the final state also gave similar oscillations, which suggests that the oscillations are independent of the accuracy of the final state. These results indicated that the oscillations originate from the interference of photoelectron waves emanating from the 60 carbon atoms, i.e., the multicentered photoemission with the phase difference of each wave. Further, the analytical calculation with a simplified spherical-shell-like initial state revealed that the spherical structure of C_{60} molecule and its large radius dominate the oscillations. [S0163-1829(98)04431-2]

I. INTRODUCTION

Because of the unique molecular structure like a spherical shell, C_{60} has attracted much interest and its electronic structure has been extensively studied.[1–5] Ultraviolet photoelectron spectroscopy (UPS) offers detailed information on the electronic structure of valence states, and many studies on C_{60} have been carried out.[6–8] Recently, much attention has been paid to the phenomenon observed by Benning *et al.* for thin films of C_{60}.[9] The photoemission intensities of the highest occupied molecular orbital (HOMO) and the next-HOMO (NHOMO) states exhibit remarkable oscillations with the incident photon energy in the range of $h\nu = 10-120$ eV. Such oscillation has not been observed in other molecular solids. Since the symmetry of the HOMO and NHOMO states is odd (ungerade) and even (gerade), respectively, and the oscillation of each state shows an opposite phase, they mentioned that the final states retain the distinct molecular character and symmetry, and the oscillations can be qualitatively explained by the parity selection rule. Wu *et al.* also reported the corresponding intensity oscillations in the single crystal of C_{60}.[10] In addition to the discussion about the selection rule, they pointed out that the final-state effects are very strong in C_{60}. The gas phase UPS measurements of C_{60} were carried out by Liebsh *et al.* and the oscillations found in the solid phase were also observed.[11]

From theoretical points of view, Xu, Tan, and Becker first reported two simple models to explain these oscillations in C_{60}.[12] They approximated the initial- (ψ_i) and final- (ψ_f) state wave functions as $\psi_i = R_{l_i}(r) Y_{l_i m_i}(\theta, \phi)$ and $\psi_f = R_{l_f}(r) Y_{l_f m_f}(\theta, \phi)$ with the radial and angular parts in the spherically symmetric potential of C_{60}, and calculated the energy positions of the cross-section minima by using one of the allowed states ($l_f = l_i - 1$). Although their calculated results matched fairly well with the observed oscillations, the approximation omitting $l_f = l_i + 1$ is rough as discussed in this paper. They concluded that the oscillations originate from a specific ability of C_{60} to form a spherical standing wave of the final state by the interference inside the molecule. As mentioned by themselves, however, more detailed and quantitative studies are required to confirm the origin of the oscillations.

We measured the angle-resolved ultraviolet photoelectron spectra (ARUPS) of C_{60} thin films in the photon-energy range of $h\nu = 18-110$ eV, and calculated the $h\nu$ dependences of the differential photoionization cross sections by changing the degree of approximation for the final and initial states. First we carried out the numerical calculations by the single-scattering approximation for the final state with the *ab initio* molecular orbital (MO) calculation for the initial state, where the angular parameters for the incident light and the photoelectron momentum were identical with the experimental conditions. It is noted that such quantitative calculations considering the scattering effects, to our knowledge, have not been reported yet for C_{60}. Next, we simplified only the final state, and calculated the photoionization cross sections by using the plane-wave final state. Further, we approximated the MO initial state by a spherical-shell-like state, and derived a simple formula for the differential photoionization cross section of C_{60}. The measured and these calculated results gave us a clear understanding of the origin of the oscillations.

II. EXPERIMENT

ARUPS measurements were carried out by using the synchrotron radiation source at the beamline BL8B2 of the UV-SOR storage ring in Institute for Molecular Science (IMS). In the preparation chamber (base pressure $\sim 10^{-9}$ Torr), pu-

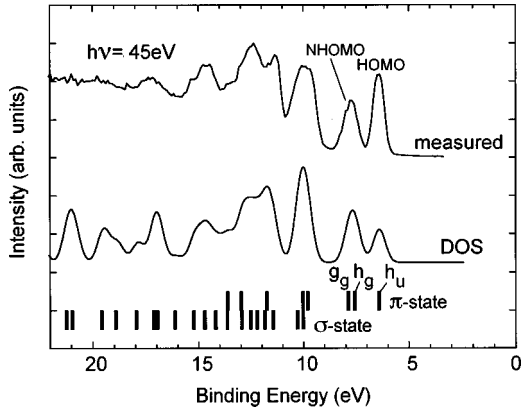

FIG. 1. Valence band ARUPS and DOS of C_{60}. The energy levels of the initial MO are shown by the longitudinal bars. The DOS curve was calculated by the Gaussian broadening of the energy levels with the width of 0.58 eV. HOMO (h_u) and NHOMO (h_g+g_g) are the π dominant states.

rified C_{60} was evaporated onto a cleaved highly oriented pyrolytic graphite substrate. The film thickness was estimated to be about 150 Å with a quartz thickness monitor. After transferring the sample film to the measurement chamber (base pressure $\simeq 4\times10^{-10}$ Torr), the ARUPS were measured at room temperature with varying the incident photon energy in the range of $h\nu=18-110$ eV. The angular parameters were kept at the incidence angle of photons $\alpha=0°$ and the take-off angle of photoelectrons $\theta=50°$ measured from the surface normal. The calculations of $h\nu$ dependences of ARUPS were carried out on the IBM SP2 computer at the Computer Center of IMS.

III. RESULTS AND DISCUSSION

A. Measured ARUPS

The upper spectrum in Fig. 1 shows the measured ARUPS of C_{60} thin film at the photon energy $h\nu=45$ eV. The HOMO and NHOMO bands are observed separately from the other valence bands. Despite the fact that the spectrum was measured in the solid phase, the distinct band shape of each band is similar to that observed in the spectra of gas phase C_{60}.[11] This similarity suggests the weakness of the intermolecular interaction of C_{60} in the thin film. The lower curve in Fig. 1 shows the calculated density of states (DOS). The longitudinal bar represents the binding energy E_b of each state calculated by the STO-5G MO method.[13] The Gaussian broadening of each state with the width of 0.58 eV gives the DOS curve, where 0.58 eV came from the observed bandwidth of the HOMO state. The DOS curve corresponds well with the measured ARUPS and indicates that the π dominant HOMO and NHOMO states are made up of h_u and h_g+g_g orbitals in I_h point group, respectively. Although the quantitative comparison with ARUPS should be made by the photoemission intensities as previously reported by us,[14–16] we used here the DOS curve only to examine the accuracy of the present MO calculation for the initial state.

Figure 2 shows the measured $h\nu$ dependence of ARUPS on the thin films of C_{60} in the binding energy region of 4.5–9 eV. The spectrum at each $h\nu$ was normalized by the peak area of the NHOMO band that was estimated by the least-square fit with a Gaussian function. The HOMO band exhibits a remarkable intensity variation with maxima and minima in the photon-energy region of $h\nu=18-110$ eV, which is almost the same as reported previously.[9–11] In the next section, the measured $h\nu$ dependence is quantitatively studied by the comparison with the calculated photoemission intensities.

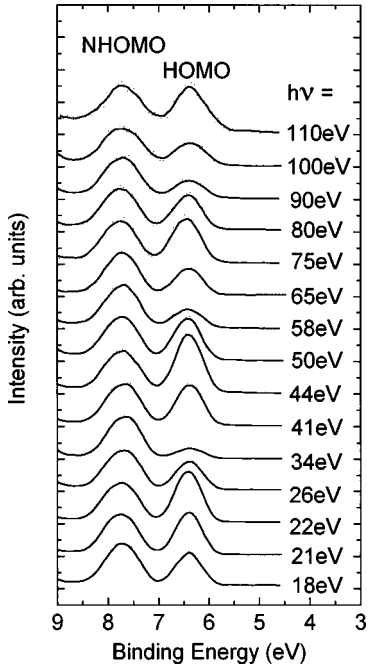

FIG. 2. Measured ARUPS of thin films of C_{60} in the photon-energy region of $h\nu=18-110$ eV. The incidence angle of photons $\alpha=0°$, and the take-off angle of photoelectrons $\theta=50°$.

B. Comparison between calculated and measured photoemission intensities

The basic ARUPS theory by considering the single and multiple scattering effects was already developed in detail.[17,18] We have modified their formula for the weakly interacting molecular solids within the single-scattering approximation for the final state,[14] and the differential photoionization cross section $d\sigma_n(\mathbf{k}_n)/d\hat{\mathbf{r}}$ of the nth molecular orbital at the given incident photon energy $h\nu$ is represented by

$$d\sigma_n(\mathbf{k}_n)/d\hat{\mathbf{r}}\propto k_n h\nu|A^n_{\mathrm{tot}}(\mathbf{k}_n)|^2, \tag{1}$$

$$A^n_{\mathrm{tot}}(\mathbf{k}_n)\propto\sum_a\sum_{Xa} D_a C^n_{Xa} e^{-i\mathbf{k_n}\cdot\mathbf{R}_a}\sum_L Y^*_L(\hat{\mathbf{R}})M_{LXa} + \sum_a\sum_{b\neq a}\sum_{Xa} D_b C^n_{Xa} e^{-i\mathbf{k_n}\cdot\mathbf{R}_b}\sum_L\sum_{L'} Y^*_{L'}(\hat{\mathbf{R}}) \times t^{l'}_b(k_n)G_{L'L}(\mathbf{R}_b-\mathbf{R}_a)M_{LXa}, \tag{2}$$

$$M_{LXa}(k_n)=-(-i)^l e^{i\delta^a_l}\rho^a_l(k_n)\int Y_L(\hat{\mathbf{r}})\hat{\epsilon}\cdot\hat{\mathbf{r}}Y_{Xa}(\hat{\mathbf{r}})d\hat{\mathbf{r}}, \tag{3}$$

$$\rho_l^a(k_n)=\int R_l(k_nr)f_{la}(r)r^3dr, \tag{4}$$

$$Y_{Xa}(\hat{\mathbf{r}})=\sum_{ma} n(m_a)Y_{La}(\hat{\mathbf{r}}), \tag{5}$$

$$t_b^{l'}(k_n)=-(e^{2i\delta_{l'}^b}-1)/2ik_n, \tag{6}$$

$$G_{L'L}(\mathbf{R}_b-\mathbf{R}_a)=-4\pi ik_n \times\sum_{L''}(-i)^{l''}(-1)^{l-l'+m'}h_{l''}^{(1)}(k_nR_{ab}) \times Y_{L''}(\hat{\mathbf{R}}_{ab})\int Y_L(\hat{\mathbf{r}})Y_{L''}(\hat{\mathbf{r}})Y_{l'-m'}(\hat{\mathbf{r}})d\hat{\mathbf{r}}, \tag{7}$$

where $\mathbf{k}_n$ $(=k_n\hat{\mathbf{R}})$ is the photoelectron wave vector, $\hat{\mathbf{R}}$ is the direction of detector, and the origin of $\mathbf{r}$ $(=r\hat{\mathbf{r}})$ is put on the center of each atom. The angular momenta of the initial and final states are denoted by $L_a=(l_a,m_a)$ and $L=(l,m)$, respectively. C_{Xa}^n is the nth molecular orbital coefficient of the Slater-type atomic orbital Xa $(=s,p_x,p_y,p_z)$, and $\mathbf{R}_a$ is the position of the atom a. M_{LXa} corresponds to the matrix element that includes the phase shift δ_l^a and radial integral $\rho_l^a(k_n)$ calculated in the muffin-tin potentials. $R_l(k_nr)$ is the radial part of the final wave function, and $f_{la}(r)$ is the radial part of the initial atomic wave function. $t_b^{l'}(k_n)$ and $G_{L'L}(\mathbf{R}_b-\mathbf{R}_a)$ are the single-scattering vertex and the free propagator, respectively. The first term in Eq. (2) represents the self-scattering wave emanating from each atomic site, where the summation with a is carried out over all atoms in a molecule. This term corresponds to the formula by the independent atomic center approximation.[19–21] The second term represents the single-scattering waves from the atom b in the molecule and the other neighboring molecules. D_a is the phenomenological damping factor due to the inelastic effects in the solid, which involves the mean free path of photoelectron.[22] k_n is related to the photoelectron kinetic energy E_k $(=h\nu-E_b)$ and inner potential V_0 by $k_n=\sqrt{2m(E_k-V_0)}/\hbar$.

The differential photoionization cross section with the plane-wave final state, $d\sigma_n^{pw}(\mathbf{k}_n)/d\hat{\mathbf{r}}$, is given by substituting $\delta_l^a=\delta_l^b=0$ into Eqs. (3) and (6) and using the spherical Bessel function $j_l(k_nr)$ instead of $R_l(k_nr)$. Thus we obtain

$$d\sigma_n^{pw}(\mathbf{k}_n)/d\hat{\mathbf{r}} \propto k_nh\nu\left|\sum_a\sum_{Xa} D_aC_{Xa}^n e^{-i\mathbf{k_n}\cdot\mathbf{R}_a}\sum_L Y_L^*(\hat{\mathbf{R}})M_{LXa}^{pw}\right|^2, \tag{8}$$

$$M_{LXa}^{pw}(k_n)=-(-i)^l\rho_l^{a,pw}(k_n)\int Y_L(\hat{\mathbf{r}})\hat{\epsilon}\cdot\hat{\mathbf{r}}Y_{Xa}(\hat{\mathbf{r}})d\hat{\mathbf{r}}, \tag{9}$$

$$\rho_l^{a,pw}(k_n)=\int j_l(k_nr)f_{la}(r)r^3dr. \tag{10}$$

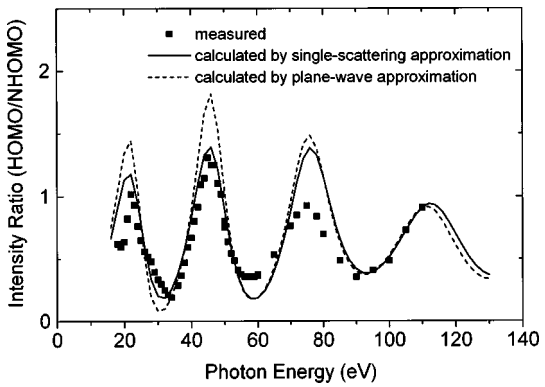

FIG. 3. Photon energy $h\nu$ dependences of photoemission intensity ratio of HOMO/NHOMO. The intensity oscillation of the measured results (solid squares) is in good agreement with the calculated curves. The solid line was calculated by the single-scattering approximation for the final state. The broken line was calculated by the plane-wave approximation for the final state. The initial state calculated by STO-5G MO method was used for both calculations.

In the plane-wave approximation, the potential by the surrounding atoms has no effect on the emitting photoelectrons. When the kinetic energy of photoelectrons is as low as in the present experiment, such approximation is too simple to calculate the differential photoionization cross section. However, we did use it to indicate that the oscillations are independent of the accuracy of the final state.

By using the equations for $d\sigma_n(\mathbf{k}_n)/d\hat{\mathbf{r}}$ and $d\sigma_n^{pw}(\mathbf{k}_n)/d\hat{\mathbf{r}}$, we calculated the $h\nu$ dependences of photoemission intensity for the HOMO and NHOMO bands of C_{60}. At room temperature C_{60} molecule is rotating freely even in the solid phase.[23] Therefore, we carried out the calculations for 500 random molecular orientations with the experimental angular parameters $\alpha=0°$ and $\theta=50°$, and averaged these results for the case of the rotating molecule.[24] The values of C_{Xa}^n and E_b for each band were obtained by the STO-5G MO calculation.[13] Since the damping effect of photoelectrons by D_a was not so considerable in the present calculations, the following results were obtained without considering this effect.

In Fig. 3, the measured and calculated $h\nu$ dependences of the intensity ratio, HOMO/NHOMO, are shown. The solid squares are the measured result, which includes the data in Fig. 2 and the additional results at the other photon energies. They show the similar oscillation as reported previously for energy positions of the maxima and minima,[9,10] while the intensity ratio is slightly different. The latter is caused by the different experimental conditions for α and θ. The solid curve represents the calculated intensity ratio by the single-scattering approximation, where the scattering waves from the three neighbor atoms (nearest and second-nearest atoms) in the molecule were considered. It reproduces the measured energy positions of the maxima and minima reasonably well. The broken curve represents the calculated result by the plane-wave approximation. It also agrees with the measured oscillation for the energy positions. As shown in Fig. 3, the period of the energy positions of the maxima and minima is not constant but increases with $h\nu$. In both calculations, the inner potential V_0 was used as an adjustable parameter. The change of V_0 causes only the shift of the energy positions

without changing the period of them. In the present experiment, the best fit between the measured and calculated results was obtained with $V_0=-13$ eV, which gives a rough estimate of the inner potential for the photoionization of the C_{60} film. In the low photon energy of $h\nu=18-55$ eV, a better agreement for the intensity ratio is obtained by the single-scattering approximation than by the plane-wave approximation. This is reasonable, since the scattering effect of a lower-energy photoelectron is not negligible to calculate the photoionization cross section quantitatively.[17,18] The disagreement of the calculated intensity ratio with the measured results is found for $h\nu=55-90$ eV, but at present we have no reliable reason for it.

Both $d\sigma_n(\mathbf{k}_n)/d\hat{\mathbf{r}}$ and $d\sigma_n^{pw}(\mathbf{k}_n)/d\hat{\mathbf{r}}$ are based on the interference of photoelectron waves, since they are made up of a sum of the individual photoelectron wave from each atomic site $\mathbf{R}_a$ with its phase difference. It is mainly caused by the factor $e^{-i\mathbf{k_n}\cdot\mathbf{R}_a}$, and $\mathbf{k_n}$ depends on the incident photon energy $h\nu$. By changing the phase difference with $h\nu$, an oscillation can occur in the calculation. Therefore, the agreement between the calculated and measured results in Fig. 3 suggests that the oscillation originates from the interference of photoelectron waves emanating from each atom constituting the C_{60} molecule, i.e., the multicentered photoemission from the MO state. Further, it should be noted that the calculated result by the simplest plane-wave approximation for the final state exhibits the similar oscillation as the measured one. This points out that the oscillation itself is independent of the accuracy of the final state. It should be ruled by a specific character of the initial state due to the molecular geometry of C_{60}. We will clarify this point in the next section.

C. Simplified analytical calculation of photoemission intensities

The specific character of the initial state in C_{60} can be understood by the following analytical calculation by simplifying the initial MO state to a spherical-shell-like state. The formula of $d\sigma_n^{pw}(\mathbf{k}_n)/d\hat{\mathbf{r}}$ in Eq. (8) is rearranged by using $d\mathbf{r}=r^2dr\ d\hat{\mathbf{r}}$,

$$d\sigma_n^{pw}(\mathbf{k}_n)/d\hat{\mathbf{r}}\propto k_n h\nu\left|\sum_a \int e^{-i\mathbf{k_n}\cdot\mathbf{R}_a} \times\sum_L (-i)^l j_l(k_n r)Y_L^*(\hat{\mathbf{R}})Y_L(\hat{\mathbf{r}}) \times\hat{\boldsymbol{\epsilon}}\cdot\mathbf{r}\sum_{Xa} C_{Xa}^n f_{la}(r)Y_{Xa}(\hat{\mathbf{r}})d\mathbf{r}\right|^2. \quad (11)$$

Using the expansion of a plane wave $e^{-i\mathbf{k_n}\cdot\mathbf{r}}=4\pi\Sigma_L(-i)^l j_l(k_n r)Y_L^*(\hat{\mathbf{k}})Y_L(\hat{\mathbf{r}})$ and $\hat{\mathbf{k}}=\hat{\mathbf{R}}$, Eq. (11) becomes

$$d\sigma_n^{pw}(\mathbf{k}_n)/d\hat{\mathbf{r}}\propto k_n h\nu\left|\sum_a \int e^{-i\mathbf{k_n}\cdot(\mathbf{r}+\mathbf{R}_a)} \times\hat{\boldsymbol{\epsilon}}\cdot\mathbf{r}\sum_{Xa} C_{Xa}^n f_{la}(r)Y_{Xa}(\hat{\mathbf{r}})d\mathbf{r}\right|^2. \quad (12)$$

By changing the origin of the wave functions from each atomic site to the center of C_{60} molecule ($\mathbf{r}\rightarrow\mathbf{r}-\mathbf{R}_a$), we obtain

$$d\sigma_n^{pw}(\mathbf{k}_n)/d\hat{\mathbf{r}}\propto k_n h\nu\left|\int e^{-i\mathbf{k_n}\cdot\mathbf{r}}\hat{\boldsymbol{\epsilon}}\cdot\mathbf{r}\psi_i(\mathbf{r})d\mathbf{r}\right|^2, \quad (13)$$

where we simplified the initial state as

$$\psi_i(\mathbf{r})=\sum_a\sum_{Xa} C_{Xa}^n f_{la}(r-R_a)\widetilde{Y_{Xa}(\mathbf{r}-\mathbf{R}_a)} \quad (14)$$

$$\simeq\Theta(r)Y_{L_i}(\hat{\mathbf{r}}). \quad (15)$$

Equation (14) is the expression of the linear combination of atomic orbital (LCAO) MO. Since the I_h group of C_{60} molecule is close to spherical symmetry, the LCAO MO is approximated with a simple spherical-shell-like state in Eq. (15), and the HOMO (h_u) and NHOMO (h_g+g_g) states are classified with the labels of $l_i=5$ and $l_i=4$.[2,3] The radial part $\Theta(r)$ of both states should have one node on the sphere surface due to the π character of both states. By substituting Eq. (15) into Eq. (13), the differential photoionization cross section becomes

$$d\sigma_n^{pw}(\mathbf{k}_n)/d\hat{\mathbf{r}}\propto k_n h\nu\left|\sum_L Y_L^*(\hat{\mathbf{R}})(-i)^l \times\int j_l(k_n r)\Theta(r)r^3dr\int Y_L(\hat{\mathbf{r}})\hat{\boldsymbol{\epsilon}}\cdot\hat{\mathbf{r}}Y_{L_i}(\hat{\mathbf{r}})d\hat{\mathbf{r}}\right|^2. \quad (16)$$

The integral of the angular part gives the selection rule of $l=l_i\pm1$, and the right-hand side of Eq. (16) can be expanded to

$$k_n h\nu\left|(-i)^{l_i+1}\int j_{l_i+1}(k_n r)\Theta(r)r^3dr \times\sum_m Y_{L_i+1}^*(\hat{\mathbf{R}})\int Y_{L_i+1}(\hat{\mathbf{r}})\hat{\boldsymbol{\epsilon}}\cdot\hat{\mathbf{r}}Y_{L_i}(\hat{\mathbf{r}})d\hat{\mathbf{r}} +(-i)^{l_i-1}\int j_{l_i-1}(k_n r)\Theta(r)r^3dr\sum_m Y_{L_i-1}^*(\hat{\mathbf{R}}) \times\int Y_{L_i-1}(\hat{\mathbf{r}})\hat{\boldsymbol{\epsilon}}\cdot\hat{\mathbf{r}}Y_{L_i}(\hat{\mathbf{r}})d\hat{\mathbf{r}}\right|^2. \quad (17)$$

Further, the following approximation of spherical Bessel function $j_l(k_n r)$ is made under the present experimental conditions. Considering the experimental photon-energy range and C_{60} radius, $k_n r$ should be about 8–20. In this $k_n r$ range, the well-known asymptotic form of spherical Bessel function for $k_n r\rightarrow\infty$ is not adequate. Therefore, we modified the asymptotic form with a correction factor α_{l_i} as

$$j_{l_i+1}(k_n r)=\frac{1}{k_n r}\cos\left\{k_n r+\alpha_{l_i}-\frac{[(l_i+1)+1]}{2}\pi\right\}, \quad (18)$$

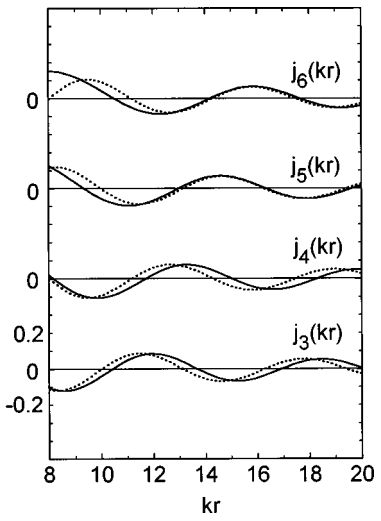

FIG. 4. Exact spherical Bessel functions and approximated asymptotic functions. The used correction factors α_{l_i} are $\alpha_5=1.4$ for $j_6(k_nr)$ and $j_4(k_nr)$ and $\alpha_4=1.0$ for $j_5(k_nr)$ and $j_3(k_nr)$.

$$j_{l_i-1}(k_nr)=\frac{1}{k_nr}\cos\left\{k_nr+\alpha_{l_i}-\frac{[(l_i-1)+1]}{2}\pi\right\}. \tag{19}$$

Figure 4 shows the comparison between the exact spherical Bessel functions and the approximated ones in Eqs. (18) and (19). $j_6(k_nr)$ and $j_4(k_nr)$ in Fig. 4 are the terms used for HOMO ($l_i=5$) with the correction factor $\alpha_5=1.4$. $j_5(k_nr)$ and $j_3(k_nr)$ are for NHOMO ($l_i=4$) with $\alpha_4=1.0$. The approximated curves (broken lines) coincide fairly well with the exact functions (solid lines) in the present k_nr region. In the previous photoionization cross section calculation for C_{60}, Xu, Tan, and Becker neglected the term of $l=l_i+1$, because the amplitude of the final wave function for very large l should be small.[12] This approximation may not be applicable for the present case as seen in Fig. 4, where the amplitude of $j_{l_i+1}(k_nr)$ and $j_{l_i-1}(k_nr)$ is comparable. Substituting Eqs. (18) and (19) into Eq. (17), we have the approximated form of

$$\begin{aligned}d\sigma_n^{pw}(\mathbf{k}_n)/d\hat{\mathbf{r}}\propto k_n h\nu\\ \times\left\{\int\frac{1}{k_nr}\cos\left(k_nr+\alpha_{l_i}-\frac{l_i}{2}\pi\right)\Theta(r)r^3dr\right\}^2\\ \times\left|\sum_m Y^*_{L_i+1}\int Y_{L_i+1}\hat{\boldsymbol{\epsilon}}\cdot\hat{\mathbf{r}}Y_{L_i}d\hat{\mathbf{r}}\right.\\ \left.+\sum_m Y^*_{L_i-1}\int Y_{L_i-1}\hat{\boldsymbol{\epsilon}}\cdot\hat{\mathbf{r}}Y_{L_i}d\hat{\mathbf{r}}\right|^2.\end{aligned} \tag{20}$$

Since the angular term $|\Sigma_m\cdots+\Sigma_m\cdots|^2$ is independent of k_n, it only contributes to the photon-energy dependence of the cross section as a constant. Thus, we obtain the simple equation for the differential photoionization cross section,

$$d\sigma_n^{pw}(\mathbf{k}_n)/d\hat{\mathbf{r}}\propto\frac{h\nu}{k_n}\left\{\int\cos\left(k_nr+\alpha_{l_i}-\frac{l_i}{2}\pi\right)\Theta(r)r^2dr\right\}^2. \tag{21}$$

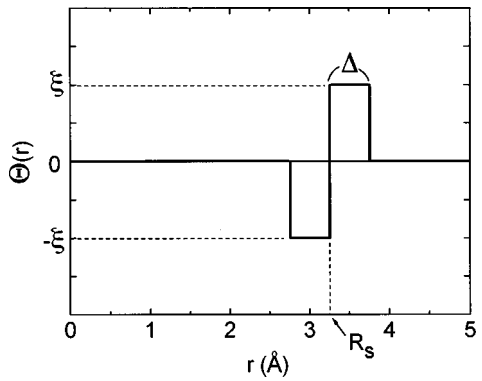

FIG. 5. An approximated radial wave function $\Theta(r)$. To simplify the present calculation, it has nonzero value for $r=R_s-\Delta\sim R_s+\Delta$. The node at $r=R_s$ is due to the π character of the HOMO and NHOMO states.

In order to evaluate Eq. (21) by a simple analytical calculation, we approximate the radial part of initial state $\Theta(r)$ by step functions as shown in Fig. 5,

$$\Theta(r)=\begin{cases}-\xi, & R_s-\Delta\leqslant r\leqslant R_s\\ \xi, & R_s\leqslant r\leqslant R_s+\Delta\end{cases}. \tag{22}$$

R_s and Δ stand for the radius of the node in the spherical shell and the half width of the shell, respectively. Consequently, the integral in Eq. (21) is easily solved and the differential photoionization cross section at a given photon energy $h\nu$ can be calculated.

In Fig. 6, the calculated $h\nu$ dependences of the photoionization cross section for the HOMO and NHOMO states are plotted with E_k. The solid curves are the results by the spherical-shell-like initial state and the plane-wave final state, where we used the parameters $R_s=3.26$ Å, $\Delta=0.5$ Å, and $V_0=-10$ eV. The values are reasonable, since $R_s=3.26$ Å is close to 3.54 Å of the radius of C_{60}, and $\Delta=0.5$ Å was referred to the average half thickness of the

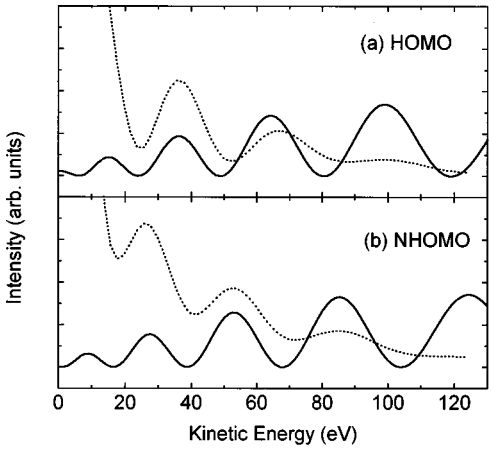

FIG. 6. Calculated $h\nu$ dependences of photoionization cross section. The solid curves were calculated with the spherical-shell-like initial state and the plane-wave final state, where $R_s=3.26$ Å, $\Delta=0.5$ Å, and $V_0=-10$ eV. The broken curves were calculated by the STO-5G MO initial state and the single-scattering final state corresponding to the solid curve in Fig. 3. The results for (a) HOMO and (b) NHOMO states are plotted with E_k.

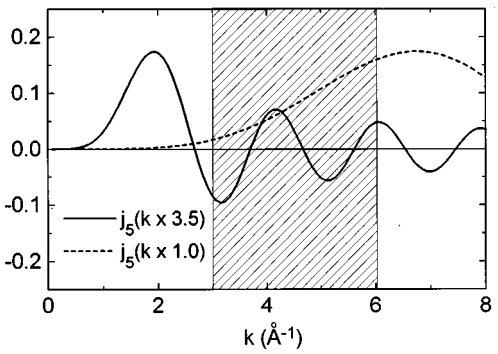

FIG. 7. Molecular size dependence of spherical Bessel function $j_l(k_n r)$. The functions for the different r value, $j_5(k_n \times 3.5)$ and $j_5(k_n \times 1.0)$, are plotted. The k_n range under the present experimental conditions was about $3-6\ \text{Å}^{-1}$ (shadowed region).

deep potential shell for carbon solids,[25] and $V_0 = -10$ eV is almost similar to the typical value estimated in other organic solids.[26,27] The broken curves are the same results as shown in Fig. 3 calculated by the STO-5G MO initial state and the single-scattering final state. Note that the broken curves represent the intensity oscillations for the HOMO and NHOMO states before deriving their ratio in Fig. 3. In spite of the present rough approximations for the initial and final states, the simple calculations with Eqs. (21) and (22) give the equal oscillations as obtained by the more sophisticated calculations in regard to the energy positions of maxima and minima for both states.[28] It means that the simplest model contains an essential point for the oscillations, that is, the spherical-shell-like initial state due to the specific structure of C_{60} dominates the oscillations.

In addition, the radius of the spherical shell is also important to observe the oscillations in the experimental $h\nu$ range. In order to demonstrate this point, we roughly examine Eq. (21) for the following cases, (i) $\Theta(r)$ has a nonzero value around $r = 3.5$ Å and (ii) it has a nonzero value around $r = 1.0$ Å. The former is for the case of a large spherical-shell molecule like C_{60}, while the latter is for a smaller shell, which may correspond to usual organic molecules. Note that $\Theta(r)$ does not need to have a node on the sphere. Since the oscillation derived by Eq. (21) is due to the cosine term, $\cos(k_n \times 3.5 + \text{const})$ and $\cos(k_n \times 1.0 + \text{const})$ are picked out for the examination. k_n varies in the range of $3-6\ \text{Å}^{-1}$ under the present experimental conditions. In this k_n range, the cosine term for $r = 3.5$ Å decreases and increases across 0 and an oscillation will be observed in $d\sigma_n^{pw}(\mathbf{k}_n)/d\hat{\mathbf{r}}$. On the other hand, the cosine term for $r = 1.0$ Å is hardly changed due to the longer period of the cosine term, and no oscillation will appear. The cosine term came from the approximation of the spherical Bessel functions $j_l(k_n r)$ in Eqs. (18) and (19). Thus, the same change can appear in $j_l(k_n r)$ as shown in Fig. 7, where $j_5(k_n \times 3.5)$ and $j_5(k_n \times 1.0)$ are plotted as an example. $j_5(k_n \times 3.5)$ shows an apparent oscillation in the rage of $k_n = 3-6\ \text{Å}^{-1}$ (shadowed region), whereas j_5 $(k_n \times 1.0)$ shows no oscillation. Therefore, it is concluded that the essential factors for the oscillations are (1) the molecular structure of C_{60} like a spherical shell, and (2) the fairly large radius of the shell.

IV. CONCLUDING REMARKS

The $h\nu$ dependences of photoemission intensities of C_{60} were calculated by the single-scattering approximation and plane-wave approximation with the *ab initio* molecular orbital calculation. To our knowledge, this quantitative calculation is the first example for C_{60}. Although the calculated results by both approximations were in good agreement with the measured intensity oscillation for the energy positions of maxima and minima, the single-scattering approximation should be used for the quantitative agreement of the intensity ratio. The comparison between the calculated and measured results suggested that the oscillations observed in C_{60} originate from the interference of photoelectron waves emanating from the 60 carbon atoms constituting the molecule due to the phase difference of each wave. The simple analytical calculation with the plane-wave final state and the spherical-shell-like initial state revealed that the essential factors for the oscillations are the spherical structure of C_{60} molecule and its fairly large radius. The importance of the spherical structure of C_{60} was already pointed out by Xu, Tan, and Becker.[12] In addition to this, we found that the large radius of C_{60} makes the oscillation observable in the present $h\nu$ range.

The observed photoemission intensity oscillations in C_{60} may not be unusual. If a molecule has a nearly spherical structure with a large radius, an intensity oscillation will be expected. To confirm this point, the measurements of $h\nu$ dependence of ARUPS for other nearly spherical molecules as carboranes, higher fullerenes, and metallocenes are in progress.

ACKNOWLEDGMENTS

The authors thank Professor Takashi Fujikawa of Chiba University for support in calculating the phase shifts of the continuum states. They also thank Professor Nobuhiro Kosugi of IMS for help in the STO-5G molecular orbital calculation. The authors thank the Computer Center of IMS, for the use of the IBM SP2 computer. This work was supported in part by Grants-in-Aid for Scientific Research (07NP0301, 07640782, and 08455004) from the Ministry of Education, Science, Sports and Culture of Japan and by Shimadzu Science Foundation.

*Present address: Institute for Molecular Science, Myodaiji, Okazaki 444, Japan.

[1] A. Oshiyama, S. Saito, N. Hamada, and Y. Miyamoto, J. Phys. Chem. Solids **53**, 1457 (1992).

[2] J. L. Martins, N. Troullier, and J. H. Weaver, Chem. Phys. Lett. **180**, 457 (1991).

[3] R. C. Haddon, L. E. Brus, and K. Raghavachari, Chem. Phys. Lett. **125**, 459 (1986).

[4] M. Ozaki and A. Takahashi, Chem. Phys. Lett. **127**, 242 (1986).

[5] R. Saito, G. Dresselhaus, and M. S. Dresselhaus, Phys. Rev. B **46**, 9906 (1992).

[6] J. H. Weaver, J. Phys. Chem. Solids **53**, 1433 (1992).

[7] T. Takahashi, S. Suzuki, T. Morikawa, H. Katayama-Yoshida, S. Hasegawa, H. Inokuchi, K. Kikuchi, S. Suzuki, K. Ikemoto, and Y. Achiba, Phys. Rev. Lett. **68**, 1232 (1992).

[8] S. Hino, K. Matsumoto, S. Hasegawa, K. Iwasaki, K. Yakushi, T.

Motikawa, T. Takahashi, K. Seki, K. Kikuchi, S. Suzuki, I. Ikemoto, and Y. Achiba, Phys. Rev. B **48**, 8418 (1993).

[9] P. J. Benning, D. M. Poirier, N. Troullier, J. L. Martins, J. H. Weaver, R. E. Haufler, L. P. F. Chibante, and R. E. Smalley, Phys. Rev. B **44**, 1962 (1991).

[10] J. Wu, Z. X. Shen, D. S. Dessau, R. Cao, D. S. Marshall, P. Pianetta, I. Lindau, X. Yang, J. Terry, D. M. King, B. O. Wells, D. Elloway, H. R. Wendt, C. A. Brown, H. Hunziker, and M. S. de Vries, Physica C **197**, 251 (1992).

[11] T. Liebsch, O. Plotzke, F. Heiser, U. Hergenhahn, O. Hemmers, R. Wehlitz, J. Viefhaus, B. Langer, S. B. Whitfield, and U. Becker, Phys. Rev. A **52**, 457 (1995).

[12] Y. B. Xu, M. Q. Tan, and U. Becker, Phys. Rev. Lett. **76**, 3538 (1996).

[13] N. Kosugi, Library Program GFCF3 (The Computer Center, The University of Tokyo, 1985). In order to fit with the measured spectra, the energy scale of DOS was contracted and shifted ($E\times 0.7+2.4$) from the results of the STO-5G MO calculation.

[14] S. Hasegawa, H. Inokuchi, K. Seki, and N. Ueno, J. Electron Spectrosc. Relat. Phenom. **78**, 391 (1996).

[15] N. Ueno, J. Electron Spectrosc. Relat. Phenom. **78**, 345 (1996).

[16] N. Ueno, A. Kitamura, K. K. Okudaira, T. Miyamae, Y. Harada, S. Hasegawa, H. Ishii, H. Inokuchi, T. Fujikawa, T. Miyazaki, and K. Seki, J. Chem. Phys. **107**, 2079 (1997).

[17] A. Liebsch, Phys. Rev. B **13**, 544 (1976).

[18] T. Fujikawa, J. Phys. Soc. Jpn. **50**, 1321 (1981).

[19] W. D. Grobman, Phys. Rev. B **17**, 4573 (1978).

[20] N. J. Shevchik, J. Phys. C **11**, 3521 (1978).

[21] S. Hasegawa, S. Tanaka, Y. Yamashita, H. Inokuchi, H. Fujimoto, K. Kamiya, K. Seki, and N. Ueno, Phys. Rev. B **48**, 2596 (1993).

[22] S. Tamura, C. J. Powell, and D. R. Penn, Surf. Interface Anal. **17**, 911 (1991).

[23] R. Tycko, G. Dabbagh, R. M. Fleming, R. C. Haddon, A. V. Makhija, and M. Zahurak, Phys. Rev. Lett. **67**, 1886 (1991).

[24] For each fixed molecular orientation, the calculated $h\nu$ dependence of photoemission intensity showed an intensity variation, but the intensity and energy positions of maxima and minima were dependent on the orientation.

[25] Y. Zhou and C. Tang, Condens. Matter News **6**, 2949 (1994).

[26] S. Hasegawa, T. Mori, K. Imaeda, S. Tanaka, Y. Yamashita, H. Inokuchi, H. Fujimoto, K. Seki, and N. Ueno, J. Chem. Phys. **100**, 6969 (1994).

[27] K. Seki, N. Ueno, U. O. Karlsson, R. Engelhardt, and E. E. Koch, Chem. Phys. **105**, 247 (1986).

[28] Since the present approximated formula of the radial part $\Theta(r)$ is far from the actual π orbital of C_{60}, it is too rough to discuss the exact photoemission intensities. This may be the reason for the intensity difference between the solid and broken curves.